ELSEVIER

Thermochimica Acta 312 (1998) 63–77

thermochimica acta

Surface acidity of metal oxides. Combined microcalorimetric and IR-spectroscopic studies of variously dehydrated systems

Vera Bolis*, Giuseppina Cerrato, Giuliana Magnacca, Claudio Morterra

Dipartimento di Chimica IFM, Università di Torino, Via Pietro Giuria 9, I-10125 Torino, Italy

Abstract

The systematic use of CO adsorption at room temperature as a probe for (strong) Lewis acidity at the surface of a number of non-d/d^0 metal oxides of interest in catalysis is illustrated. The advantages of the combined use of adsorption microcalorimetry and IR spectroscopy in giving an exhaustive picture of the distribution of acid surface sites are stressed. The influence of the chemical nature (TiO_2, ZrO_2, HfO_2 and Al_2O_3) and of the structure (monoclinic/tetragonal for ZrO_2 and γ-/δ,θ- phase for Al_2O_3) of the metal oxide, as well as the dehydration degree of the surface and the presence of anionic (sulfates for zirconia) or cationic (ceria for alumina) surface dopants were considered. The blue shift of the stretching frequency of adsorbed CO and the adsorption enthalpy were measured. In the case of the group IV metal oxides the two parameters were found to be correlated, whereas in the case of pure Al_2O_3 no correlation was found. The peculiar behavior of alumina was interpreted on the basis of different processes occurring at the CO/Al_2O_3 interface. An endothermic reversible reconstruction of the surface was supposed to occur upon adsorption, leading to exceptionally low heat values. The presence of small amounts of cations, other than Al^{3+}, in the alumina matrix seemed to inhibit this effect. © 1998 Elsevier Science B.V.

Keywords: Surface acidity; Metal oxides; Microcalorimetric; IR-spectroscopic

1. Introduction

The knowledge of the number and strength of the sites existing at the surface of a catalyst is of paramount interest, as the first step in any catalytic reaction is the adsorption and the subsequent activation of the reactant molecules. Adsorption microcalorimetry is a useful technique to describe, in detail, the quantitative and energetic features of surface sites [1–3]. It allows, if properly arranged, the simultaneous determination of the adsorbed amounts of a suitable probe molecule and of the heat evolved at increasing surface coverage. By processing the equilibrium data obtained during a stepwise adsorption procedure, the evolution of the differential heat of adsorption with both coverage and equilibrium pressure can be drawn. Cycles of adsorption–desorption experiments can be performed in order to isolate the contribution to the overall process of the species irreversibly held at the surface [4,5]. This technique is used similarly in a number of laboratories working in the field of catalysis, as documented by Refs. [2–9]. The heat of adsorption can be reasonably taken as a measure of the bonding energy between the probe molecule and the sites at the surface of the adsorbent. The heterogeneity of the surface (structural, chemical and/or induced) can be pictured by processing the overall set of combined volumetric and calorimetric data.

In order to better illustrate the nature of the bonds established between the probe and the sites, calorimetry can be suitably coupled with other complemen-

*Corresponding author. Tel.: 0039 116707565; fax: 0039 116707855; E-mail: bolis@ch.unito.it

PII S0040-6031(97)00440-1

tary techniques, in particular with techniques designed to detect the chemical nature of the species present at the surface as well as the species formed at the surface upon adsorption. Infrared spectroscopy is an ideal technique for this purpose in that IR-spectroscopic data show the nature of the surface sites as well as the perturbation of the vibrational features of the adsorbed species due to the interaction with the surface. Experiments complementary and parallel to the calorimetric ones can be performed, so that both qualitative and quantitative information on the surface features (nature, population and strength of the surface sites) can be obtained [10–12]. On the other hand, the knowledge of the morphological features of the microparticles making up a powdery catalyst is very useful in describing the geometrical features of surface sites. In this respect, high-resolution electron microscopy (HRTEM) is very fruitfully combined to microcalorimetry and IR-spectroscopy. The surface properties can be correlated to the micromorphology of the particles and, in particular, to the preferentially exposed crystallographic planes and to the structural defects (steps, kink edges, etc.) at the border of the microparticles [13–17].

The recently increasing amount of computational ab initio results on species adsorbed at the surface, is ideally suited to be compared with experimental data from microcalorimetry, besides the ones obtained as isosteric heats from the isotherms [18]. The coupling of computational results with experimental calorimetric data can yield information on the nature of the interaction, either confirming the hypothesis made on the basis of experimental results, or suggesting alternative models to interpret experimental data [19].

The present contribution deals with the detailed description of the combined use of microcalorimetry and IR-spectroscopy in characterizing the bonding features of surface sites. The systematic use of carbon monoxide as a probe for the surface Lewis acidity of a number of metal oxides will be illustrated. CO is widely used as a probe molecule to characterize simple and mixed oxides, as well as cation-exchanged zeolites, thanks to its soft basic character and its relatively large polarizability, in spite of its small dipole moment (0.1 D, [20]).

Here, we briefly summarize the features of the systems studied as well as the state of art of the combined procedure. All systems studied in the present paper belong to the non-d/d^0 series of metal oxides. In such very simple systems only a plain σ-coordination is supposed to occur at room temperature on coordinatively unsaturated (CUS) cations exposed at the surface. The interaction is fully reversible and is witnessed by the appearance of reversible IR bands located at frequencies higher than that of the stretching of the C–O bond in the gas phase (ν=2143 cm^{-1}). The formation of a σ-dative bond in fact causes the ν_{CO} force constant to increase, owing to the partial emptying of the weakly antibonding 5σ lone pair orbital [21,22]. Heat of adsorption values vary in the 30–90 kJ/mol domain [8–16]. These values are reasonably ascribed to a medium-to-strong Lewis acid–base interaction and not only to a physical adsorption resulting from electrostatic and polarization forces, as occurs for block *s* metal cations [23].

The presence of different bands in the IR spectra located at ν>2143 cm^{-1}, or different components within a single complex band, reveals the heterogeneity of the CUS metal cations. Indeed, CUS metal cations can be differentiated either by their chemical nature or by their coordinative unsaturation, owing to the particular crystallographic configuration.

By adsorption calorimetry, the overall adsorption volumetric and calorimetric isotherms are obtained. On the other hand, by IR-spectroscopy the optical isotherms, defined as integrated absorbance vs. equilibrium pressure, are obtained for each adsorbed species. By comparing the overall adsorption isotherms with the optical individual ones, it is possible to obtain the molar extinction coefficient of each spectral component. The decomposition of the overall adsorption isotherms into individual components allows the population of each individual adspecies to be known and a map of the surface sites to be drawn [10,11,24–27].

In the presence of surface heterogeneity (either structural or chemical) the integral heat evolved during the adsorption process does not increase linearly with coverage, but a deviation more or less pronounced is observed. A similar deviation is also observed in the case of induced heterogeneity, due to lateral effects occurring at the surface [25,27]. As a consequence of surface heterogeneity, the differential heat of adsorption (q_{ads}) decreases with coverage. From heat of adsorption data the energy spectrum of the sites can be obtained [1,28].

Correlations do exist between spectroscopic features (spectral position ν_{CO} and molar extinction coefficient ε_{CO}) and thermodynamic ones (adsorption enthalpy $\Delta_{ads}H$ and adsorption entropy $\Delta_{ads}S$) [25,27]. In particular, the correlation between the blue-shift of the ν_{CO} stretching frequency (defined as $[\nu_{CO}]_{ads}-[\nu_{CO}]_{gas}$) and the enthalpy of adsorption, $\Delta_{ads}H$, is the most relevant one. Several attempts have been made in order to correlate the various parameters involved in the description of the interaction [22,23,29–34]. A non-linear correlation between frequency shift, molar extinction coefficient and enthalpy of adsorption [10] and a linear correlation between frequency shift and molar extinction coefficient [26] were proposed by some of us a few years ago. The non-linear correlation between spectroscopic and energetic parameters was initially proposed for a number of non-d/d^0 metal oxides, and afterwards was extended to non-d and d^{10} cations located in Y-zeolitic cavities [35].

In the present paper, we will illustrate the use of CO uptake at room temperature as a probe for the Lewis acidity of the following metal oxides: *group IV* metal oxides, TiO_2, ZrO_2 and HfO_2, in comparison with Al_2O_3. The effect of the hydration state of the surface (depending upon the activation temperature in vacuo), crystal phase of the sample (*monoclinic* and *tetragonal* for ZrO_2; γ- and δ,θ-phase for Al_2O_3) and the presence of *anionic* and *cationic* dopants in the oxidic matrix (*sulfates* in the case of ZrO_2, Ce^{4+} in the case of Al_2O_3) will be illustrated. All systems examined are of catalytic interest, either per se or as support, and for all of them surface *Lewis acidity* is an essential feature. Details on the catalytic performances are reported in Refs. [36,37] for TiO_2 and HfO_2, respectively; in Ref. [38] for *monoclinic* ZrO_2, that shows a bifunctional acid/base nature; and in Refs. [39,40] for Al_2O_3 and Al_2O_3/CeO_2, respectively. Al_2O_3/CeO_2 is widely used in automotive catalysis, but the detailed role of ceria in improving the performances of alumina has not been yet established. Particular attention will be given to sulfated zirconia ZrO_2/SO_4 that is known to possess unique catalytic properties, so that it is frequently defined as a *solid superacid* [41]. Even if the exact nature of the catalytic sites of sulfated zirconia has not been completely understood, the relevance of the presence of strong Lewis-acidic sites on the active catalyst has been demonstrated [42].

2. Experimental

2.1. Materials

- TiO_2: Crystallographically pure *anatase* preparation, obtained via sulfate procedure and thoroughly freed from sulfate impurities. N_2 BET surface area was 99 m^2/g after calcination at 773 K. See Ref. [10].
- ZrO_2: Crystallographically pure baddeleyite (*monoclinic*) preparation, obtained by the room temperature hydrolysis of zirconium isopropylate. See Ref. [11]. N_2 BET surface area was 84 m^2/g after calcination at 673 K.
- ZrO_2: Crystallographically pure *tetragonal* preparation, obtained via a sol–gel method and stabilized by the presence of 3 mol% Y_2O_3 as described in Ref. [43]. N_2 BET surface area was 85 m^2/g after calcination at 873 K.
- sulfated-ZrO_2: The sample was obtained following a procedure implying direct sulfation with H_2SO_4 of the pure *tetragonal* preparation described above, see Ref. [44]; N_2 BET surface area was 85 m^2/g and sulfates loading was 3.0 SO_4 groups/nm^2 after calcination at 923 K.
- HfO_2: Crystallographically pure *monoclinic* preparation, obtained by the room temperature hydrolysis of hafnium isopropylate, as described in Ref. [15]. N_2 BET surface area was 48 m^2/g after calcination at 773 K.
- Al_2O_3: (i) Crystallographically pure γ-phase, obtained by firing at 773 K a powdered pseudoboehmite precursor; N_2 BET surface area was 186 m^2/g, showing a porosity characterized by a pore size distribution centered ca. 32 Å; (ii) crystallographically pure δ,θ-phase, obtained by firing at 1273 K the γ-phase sample described above; N_2 BET surface area was 120 m^2/g. See Ref. [16].
- Al_2O_3/CeO_2: The sample was obtained following the same procedure adopted for γ- and δ,θ-Al_2O_3, but for adding a controlled amount of a cerium nitrate solution, in order to obtain a $CeO_2 : Al_2O_3$ ratio of 3 : 100 (2.5% wt) in the final calcined material [12,17]. N_2 BET surface areas were 159 m^2/g for γ-Al_2O_3/CeO_2 and 48 m^2/g for δ,θ-Al_2O_3/CeO_2.
- CO specpure from Matheson was employed.

- All samples were dehydrated in vacuo and oxidized in O_2 atmosphere at a chosen temperature (673, 723 and 773 K) prior to any adsorption experiment. Impurities left during the preparation were thus eliminated and the maximum stoichiometry was guaranteed to the transition metal oxides, so avoiding the presence of reduced centres.

2.2. Nomenclature

The samples examined will, hereafter, be indicated by their chemical formula, followed by a numeral indicating the activation temperature (K). For instance, *m*-ZrO_2 673 stands for a monoclinic zirconia specimen outgassed at 673; γ-Al_2O_3/CeO_2 773 stands for a ceria-doped γ-Al_2O_3 specimen outgassed at 773 K.

2.3. Methods

Microcalorimetry was employed to measure the heat of adsorption of CO in order to evaluate the enthalpy changes related to the adsorption process. A *heat-flow microcalorimeter* (standard Calvet type by Setaram, France) kept isothermally at 303 K was employed, following a well-established stepwise procedure, described in Refs. [4,10,11]. Thanks to the differential construction of the apparatus, all parasite effects other than the one due to the interaction of the gas with the surface of the solid studied could be compensated. As the process under study was fully reversible, the measured heat of adsorption corresponds to the enthalpy of adsorption ($q_{ads}=-\Delta_{ads}H$). The calorimeter was connected to a high vacuum ($p\leq10^{-6}$ torr, 1 torr=133.3 N m^{-2}) *volumetric apparatus* which enabled simultaneous determination of the adsorbed amounts (n_{ads}) and the heat evolved (Q^{int}) at increasing CO pressure (p_{CO}) for small increments of the adsorptive. The adsorbed amounts per unit surface area are reported as a function of CO pressure (volumetric isotherms, n_{ads} vs. p_{CO}) and they are taken as a direct measure of the *population* of Lewis-acidic *sites*. The population of metal cations sufficiently acidic to bind CO at room temperature is a small fraction, up to ca. 10%, of the total CUS metal cations exposed at the surface of the metal oxides studied. Thus, hereafter, we will refer to the sites adsorbing CO at room temperature as *strong* Lewis-acidic sites. The calorimetric isotherms (Q^{int} vs. p_{CO}) will not be reported for the sake of brevity. The differential heat of adsorption (q_{ads}) will be reported as a function of CO coverage (q_{ads} vs. n_{ads}). The initial heat value (q_0), corresponding to the highest energy of interaction of the probe with the strongest acidic sites, will be evaluated by extrapolating to *zero coverage* the heat vs. coverage plots.

A *first run* of adsorption was performed on the samples previously outgassed at the temperature chosen in order to reach the desired degree of dehydration of the surface. The hydration state of the surface was monitored by IR spectroscopy in the 2000–4000 cm^{-1} interval. The background spectra will not be reported for the sake of brevity. The adsorption of CO was found to be completely reversible, in that a *second run* of adsorption, performed after pumping off at the calorimeter temperature, was virtually coincident with the first one. We will thus refer to first and second runs as equivalent.

The detection threshold of the microcalorimeter is 50 μJ per impulsion. In all cases, considered in the present work, the heat evolved during the adsorption of each single dose of the adsorptive ranged 0.10–1.0 J. The pressure was measured by means of a transducer gauge (Baratron MKS, 0–100 torr).

For each dose admitted on the sample *thermokinetic* data could also be recorded. The evolution with time of the calorimetric peak was in all cases typical of an instantaneous, non-activated, molecular adsorption process. In fact, the thermogram recorded during the adsorption step of each single dose returned to the initial base-line in a time of ca. 30 min, i.e. within the time response of the heat-flow calorimeter [1].

Prior to installation into the calorimeter, each oxide sample, already located in the calorimetric cell in the form of loose powder (ca. 500–1000 mg), was outgassed at the chosen temperature. After the thermal pretreatment, the cell was isolated, cooled, and transferred into the calorimeter without further contact with the atmosphere.

IR spectra of adsorbed CO were run at 2 cm^{-1} resolution on Bruker *FTIR spectrometers* (Mod. 113 v and 88) equipped with MCT detectors. The nominal temperature was ≈300 K, but some sample heating under the IR beam has to be taken into account. Samples suitable for in situ FTIR experi-

ments were prepared either in the form of self-supporting pellets (ca. 20–30 mg/cm^2) or in the form of thin layer powder depositions (ca. 5 mg/cm^2). These latter were obtained on pure Si platelets by air-drying of water suspensions of the starting powdered material. The vacuum activated samples in a quartz cell, equipped with KBr windows, were connected to a glass vacuum line to able to reach a final residual pressure lower than 10^{-5} torr. All adsorption spectral patterns were run in a in-situ configuration, so that reliable spectral ratios and background subtractions could be obtained routinely. The contribution of the gas phase was computer subtracted from all spectra of adsorbed CO. *Spectral integrations* and *band resolutions* were carried out on unsmoothed segments of the absorbance spectra using a commercial program by Bruker (FIT) in which one only needs to set the number of spectral components and the desired accuracy. The equilibrium pressure of CO was measured by means of a Pirani gauge (p_{CO}<2 torr) or a Hg manometer (p_{CO}>2 torr). The Hg manometer allowed to measure pressures of CO as high as ≈150 torr. The accuracy was, however, lower than in the volumetric/calorimetric experiments.

3. Results and discussion

In Fig. 1, the volumetric isotherms of CO adsorbed on TiO_2, *m*-ZrO_2 and HfO_2 outgassed at T=673 K (a) and the corresponding heat of adsorption vs. coverage plots (b) are reported and compared to the ones obtained for γ-Al_2O_3 673. Considering that one CO molecule occupies one surface site upon adsorption, hereafter, we will refer to the number of adsorbed molecules as equivalent to the number of sites. Among the three *group IV* metal oxides, *m*-ZrO_2 exhibits the highest adsorption capacity, whereas HfO_2 the lowest one. The most evident feature observed in the plot is that the population of Lewis sites, sufficiently acidic to bind CO at room temperature, is much lower for *alumina* than for *group IV metal oxides*. This indicates that the dehydroxylation of the surface reached on Al_2O_3 is not as high as that reached on *group IV* metal oxides. The nature of the oxide determines the facility to the dehydroxylation. Al_2O_3 is the most ionic oxide among the four systems studied, and is the most resistant to the thermal elimination of the surface

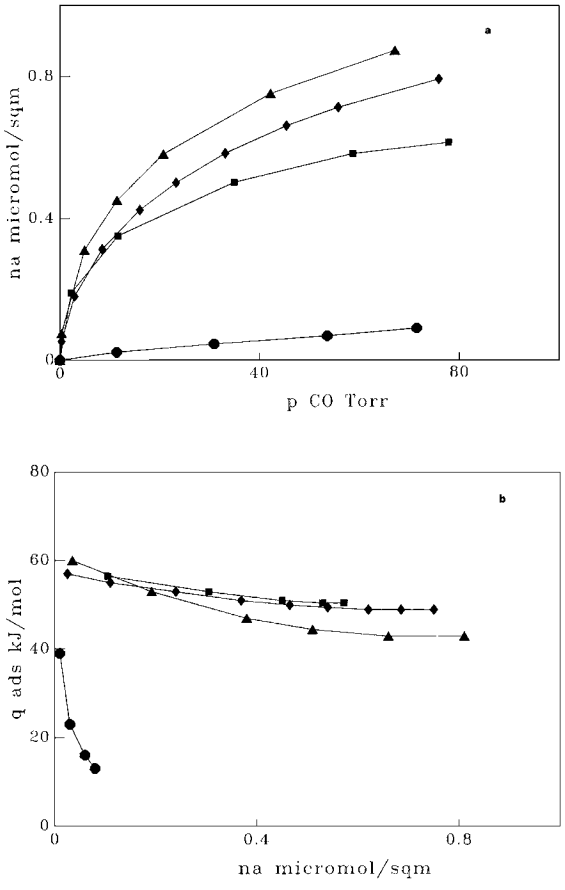

Fig. 1. (a) Adsorption volumetric isotherms of CO at 303 K on TiO_2 anatase (◆), *m*-ZrO_2 baddeleyite (▲), HfO_2 (■), and γ-Al_2O_3 (●) outgassed at 673 K. (b) Heat of adsorption as a function of CO uptake on the samples described in (a).

hydrated layer. This result confirms that different outgassing oxides at a nominally identical temperature can lead to a quite different concentration of metal cations showing Lewis acidity. This obvious consideration is, however, not always taken into account when the catalytic performances of different catalysts activated at the same temperature are compared. The structure and the chemical properties of the oxide determine the surface reconstruction. Transition aluminas are structurally complex spinel-like systems [45], involving Al^{3+} cations in both octahedral and tetrahedral coordination. Surface reconstruction is strongly affected by both crystal phase and extent of surface dehydroxylation and determines the distribution of tetrahedral CUS Al^{3+}, the ones acting as

strong Lewis-acid centers. Surface reconstruction of *group IV* metal oxides is certainly simpler than that of transition aluminas [36] and does not involve a preferential coordinative situation of the cations. ZrO_2 is more ionic than TiO_2 and the fraction of Zr^{4+} cations in high coordinative unsaturation is more abundant than on TiO_2. HfO_2 exhibits, among the three oxides of the group, the least abundant population of metal cations acting as strong Lewis acids. Its adsorption isotherm tends to reach the plateau corresponding to a CO monolayer at a pressure lower than the ones of ZrO_2 and TiO_2. The isotherms of the latter two samples still keep growing at p_{CO}>80 torr.

Also the heat of adsorption vs. coverage plots indicate a great difference between the *group IV* metal oxides and γ-Al_2O_3. First, the heat of adsorption at vanishing coverage (q_0) is ≈60 kJ/mol for TiO_2, *m*-ZrO_2 and HfO_2, with only slight differences among the three samples. Second, in all cases, q_0 is much higher than the one obtained for γ-Al_2O_3, ≈40 kJ/mol. The other relevant aspect to observe is that, while for TiO_2, *m*-ZrO_2 and HfO_2 the heat of adsorption decreases quite smoothly with coverage, in the case of Al_2O_3 the heat of adsorption decreases very steeply. The heat falls down to exceptionally low values, being q_{ads} ≈10 kJ/mol at p_{CO} ≈80 torr.

In Fig. 2, the IR spectra of CO adsorption on the samples described above are reported. In the left-hand side of the figure are shown the experimental spectra obtained at increasing CO pressure (1–150 torr). In the case of *m*-ZrO_2 and HfO_2, the right-hand side of the figure reports, as an example, two bands (at p_{CO} ≈1 torr and at p_{CO}≈150 torr) which are computer resolved into two symmetrical components. In the case of γ-Al_2O_3 only one component was present. The TiO_2 spectrum consists of two well-separated bands corresponding to two different CO adspecies, as reported and discussed extensively elsewhere [10,25]. The molar extinction coefficient values for all these σ-coordinated species are very similar, as reported in Refs. [10,24–27], and thus a semi-quantitative meaning can be attached to the intensities of the σ-coordinated CO bands. The population of the high-frequency species is very scarce, but it is predominant at very low CO pressure and saturates very quickly. So the q_0 value (≈60 kJ/mol) can be entirely ascribed to this species. More complicated is the situation for *m*-ZrO_2 and HfO_2, for which at least two bands are

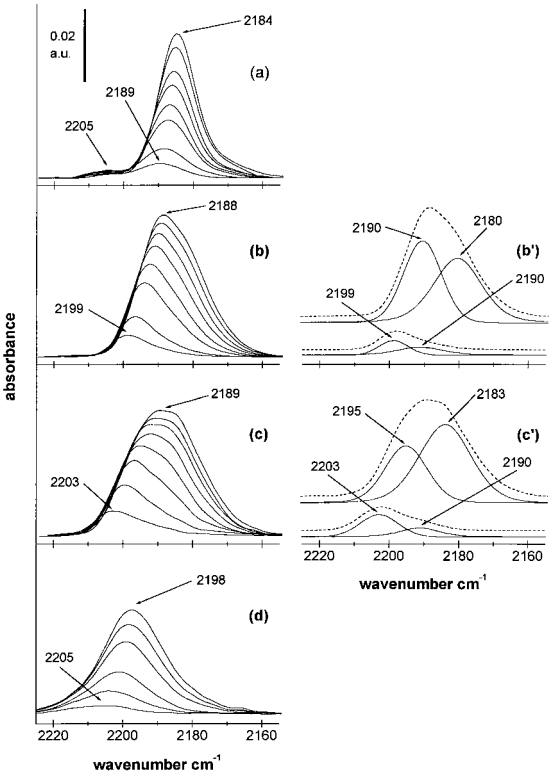

Fig. 2. IR spectra of CO adsorbed at T ≈300 K on TiO_2 anatase (a), *m*-ZrO_2 baddeleyite (b and b′), HfO_2 (c and c′) and γ-Al_2O_3 (d) outgassed at 673 K. Left side of the figure: at increasing CO pressure (1–150 torr); right side of the figure: deconvolution into single components (———) of the experimental IR bands (- - -) at p_{CO} ≈1 torr (bottom) and ≈150 torr (top). For deconvolution details, see the text.

present, but so closely overlapped that their deconvolution is rather critical. In the case of *m*-ZrO_2, (b, b′), at low CO pressure the high-frequency band (ν_{CO} ≈2199 cm^{-1}) prevails, whereas the low frequency one (located at ν_{CO} ≈2190 cm^{-1}) is much less intense. At increasing CO coverage the relative intensity of the two bands becomes comparable, and the ν_{CO} values shift to lower frequencies (ν_{CO} ≈2190 and 2180 cm^{-1}, respectively), owing to inductive effects brought about by increasing CO uptake [25–27]. It is, thus, possible for *m*-ZrO_2 to ascribe the q_0 value for the formation of the most energetic fraction of the high-frequency species, as it was done in a straightforward way for TiO_2. For HfO_2, the same procedure as for *m*-ZrO_2 was followed. The q_0 value was assigned to the high-frequency species, prevailing in the earliest stages of

the adsorption process. At high CO coverages, the low-frequency species keeps growing in intensity with respect to the high frequency one and eventually prevails, as in the case of m-ZrO_2. Both high- and low-frequency species shift downwards at increasing coverage. This effect is in line with the corresponding decrease of the heat of adsorption. In the case of TiO_2, a similar behavior is observed only for the low-frequency species. It can also be observed that, beside the close similarity of the q_0 figures for all the *group IV* metal oxides, the heat of adsorption on m-ZrO_2 decreases with coverage somewhat more steeply than on TiO_2 and HfO_2. On m-ZrO_2 the population of acidic sites is higher than that found on TiO_2 and HfO_2, but the energy distribution of the sites indicates that a fraction of the sites is slightly less acidic than those present on TiO_2 and HfO_2. The correspondent IR bands are indeed located at higher ν_{CO} frequency for TiO_2 and HfO_2 and at a slightly lower ν_{CO} for m-ZrO_2 (see Fig. 2, particularly the right-hand side). By comparing the energetic and spectroscopic data, it is observed that the correlation between ν_{CO} blue-shift and enthalpy of adsorption proposed by some of us in the past for different TiO_2 [10] preparations, is also found for m-ZrO_2 and HfO_2.

In the case of γ-Al_2O_3, the only CO species formed is located at 2205 cm^{-1} at low CO pressure and shifts to 2198 cm^{-1} at high coverage. At this stage of the process, the heat of adsorption is abnormally low (10 kJ/mol). It is very surprising and even puzzling that γ-Al_2O_3, for which the initial heat of adsorption is the lowest one among the four samples examined ($q_0 \approx 40$ kJ/mol), exhibits the highest ν_{CO} frequency at zero coverage ($\nu_0 \approx 2205$ cm^{-1}). These two data taken together do not fit at all, neither the previously proposed correlation nor the trend shown by the results obtained for the foregoing *group IV* metal oxides. The fact that transition aluminas are known as typical Lewis-acid catalysts, arouses suspicion regarding the actual meaning of the surprisingly low figure obtained for the heat of interaction. Indeed, it is the *overall heat transferred* during the contact between the gas and the solid that is *calorimetrically measured*, irrespective of how many and what kind of processes are actually occurring at the gas/solid interface. In the peculiar case of *alumina* the measured heat incorporates other processes of different nature besides the simple σ-coordination. The physical nature of this additional process causes the overall heat measured to be very low. We will come back to this result and to its interpretation after having reported the results obtained for the other Al_2O_3 samples.

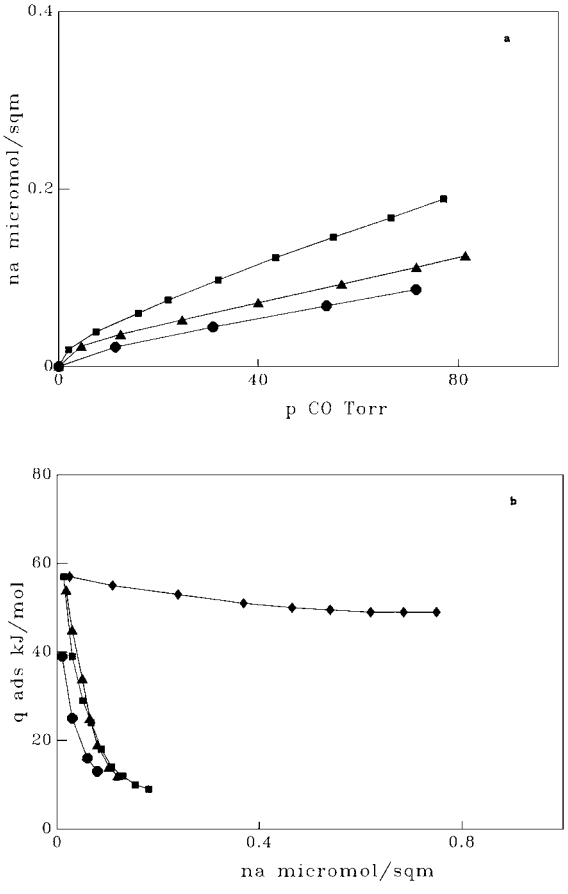

Fig. 3. (a) Adsorption volumetric isotherms of CO at 303 K on γ-Al_2O_3 outgassed at 673 K (●), on γ-Al_2O_3 outgassed at 773 K (▲) and on δ,θ-Al_2O_3 (■) outgassed at 773 K. (b) Heat of adsorption as a function of CO uptake on the samples described in (a) and compared with TiO_2 anatase outgassed at 673 K (◆).

In Fig. 3(a), the volumetric isotherms of CO adsorbed on γ-Al_2O_3 outgassed at two temperatures (673 K as reported above, and 773 K) are compared with the isotherm obtained for another transition alumina phase, namely a δ,θ-Al_2O_3 outgassed at 773 K. First, it can be observed that the increased outgassing temperature allows the number of CO sites, per unit surface area, to increase (≈33% of the sites initially present on γ-Al_2O_3 673 at $p_{CO} \approx 60$ torr). A more pronounced increase of the number of CO sites is

produced, however, by the thermal treatment at 773 K of the high temperature δ,θ-phase. The increase of the number of sites at p_{CO}=60 torr is ≈50% of the sites present on γ-Al_2O_3 773. The total amount of CO adsorbed on these samples is, however, still much lower than for TiO_2, m-ZrO_2 and HfO_2. In Fig. 3(b), the heat of adsorption vs. coverage plots for the Al_2O_3 samples just described are reported in comparison with TiO_2. It can be immediately noted that outgassing at 773 K causes, in both γ- and δ,θ-Al_2O_3, a marked increase of the initial heat of adsorption. The heat value is ≈60 kJ/mol in both cases, close to the one obtained for TiO_2. However, the similarity with TiO_2 does not concern the overall trend of the heat vs. coverage plot, in that for both γ- and δ,θ-Al_2O_3 the plots decreases steeply to very low values (≈10 kJ/mol) indicating again that something different from a plain σ-coordination does occur. In these cases, the ν_{CO} stretching frequencies are also quite high (ν_{CO}>2200 cm^{-1}). This is clearly shown in Fig. 4, where the IR spectra of CO adsorbed on γ-Al_2O_3 673 and 773 and δ,θ-Al_2O_3 773 are reported for increasing CO pressures (left-hand side). On the right-hand side of Fig. 4, an example of deconvolution of the complex experimental band of γ-Al_2O_3 773 (three species) and δ,θ-Al_2O_3 773 (two species) is shown.

The high-frequency band prevails at very low CO pressure and saturates quite quickly in both the cases, so that the initial heat of adsorption can be reasonably ascribed to the formation of the high-frequency species. At high coverages, however, the most abundant species becomes the one already present, as a single species, on γ-Al_2O_3 673 (ν_{CO} ≈2198–2200 cm^{-1}). This species was previously ascribed [16] to CO adsorbed on CUS tetrahedral Al^{3+} cations located on flat patches of low index crystal planes. The high-frequency species (ν_{CO} ≈2236 and 2218 cm^{-1}) were ascribed to CO adsorbed on CUS tetrahedral Al^{3+} cations located in the more defective crystallographic configurations, such as steps and kink edges, where the coordinative unsaturation is bound to be higher.

From the present data it is not easy to resolve energetically the two 2236 and 2218 cm^{-1} species but we can reasonably assign the *zero*-heat of adsorption (q_0 ≈70 kJ/mol) to the formation on γ-Al_2O_3 773 of the 2236 cm^{-1} species, the only one formed at low CO coverage. The 2236 cm^{-1} species is not present on

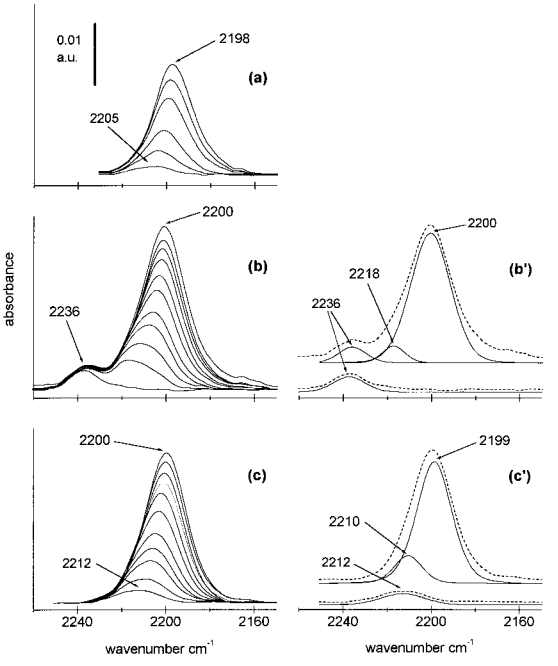

Fig. 4. IR spectra of CO adsorbed at T ≈300 K on γ-Al_2O_3 outgassed at 673 K (a), on γ-Al_2O_3 outgassed at 773 K (b and b′) and on δ,θ-Al_2O_3 (c and c′) outgassed at 773 K. Left side of the figure: at increasing CO pressure (1–150 torr); right side of the figure: deconvolution into single components (———) of the experimental IR bands (- - -) at p_{CO} ≈1 torr (bottom) and ≈150 torr (top). For deconvolution details, see the text.

the δ,θ-Al_2O_3 773 specimen discussed in the present work, but was clearly observed on δ,θ-Al_2O_3 outgassed at a higher temperature (1023 K), as reported in Ref. [16]. In this latter case the 2236 cm^{-1} band is quite intense at low CO pressure, and the relevant adspecies quite abundant. On the basis of the hypothesis that these species must contribute substantially to the heat of adsorption measured at low coverage, it was possible to assign, to the high frequency species, a q_0 ≈90 kJ/mol, and consequently a q_0 ≈70 kJ/mol to the species at 2218 cm^{-1}.

As for the rapid decrease of the heat values with coverage, observed only on transition aluminas, we refer to the following schemes for a possible explanation. Scheme 1 shows the σ-coordination of CO on a coordinatively unsaturated metal cation, the only process that is expected to occur at the surface of a non-d metal oxide.

In the case of Al_2O_3, however, different processes occur at the surface and do involve more complicated

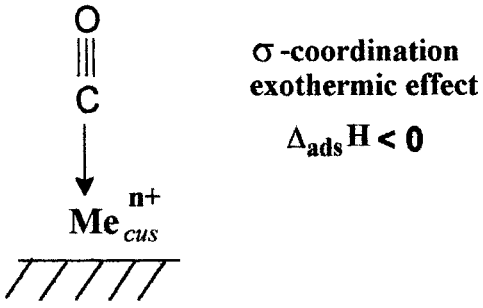

Scheme 1.

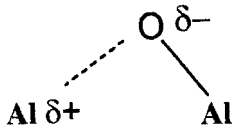

Scheme 2.

phenomena. On transition aluminas, CUS cations in strong interaction with strained Al–O bonds are abundantly present, as described in Ref. [45], and depicted in the following Scheme 2.

The adsorption of CO on the CUS Al^{3+} cations causes the interaction of these latter with the O–Al groups to be weakened, as shown in Scheme 3. As a consequence of the adsorption of CO, a modification of the surface structure is thus produced.This effect is not a mere hypothesis, but was IR-spectroscopically evidenced in the region of the Al–O modes (1100–1000 cm^{-1}) and was found to be completely reversible, as reported in Refs. [16,45,46].

From an energetic point of view, the modification of the surface requires some work to be done in order to break off the interaction between CUS Al cations and O–Al groups (see Scheme 2). Thus, the process must involve an endothermic effect ($\Delta H>0$) that, combined with the exothermic effect ($\Delta H<0$) due to the σ-coordination of CO on CUS Al^{3+} cations, results in a measured heat of interaction lower than the one expected for a plain σ-coordination. This fact can explain the lack of correlation between vibrational and energetic parameters, as well as the anomalously low heat of interaction measured in the case of Al_2O_3, never observed for other non-d/d^0 metal oxides [10,25–27].

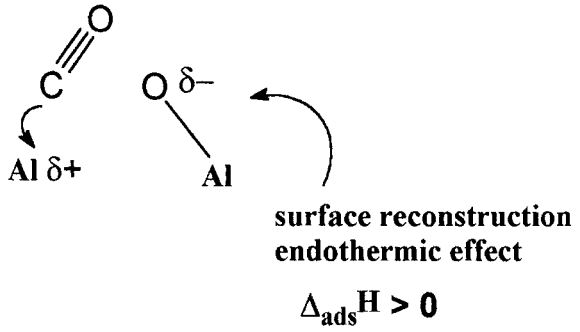

Scheme 3.

In summary, to create a high population of strong Lewis-acidic sites in *transition aluminas*, the outgassing temperature must be higher than in the case of *group IV metal oxides*. Nevertheless, the electron accepting capacity of CUS Al^{3+} cations is quite high with respect to the CUS Me^{4+} ones of the *group IV* metal oxides, as witnessed by the large blue shift of the ν_{CO} frequency. In the case of Al_2O_3, however, the heat of interaction measured for CO uptake simply cannot be taken as a measure of the electron accepting properties of CUS Al^{3+} cations, because different thermal events of opposite sign occur at the CO/Al_2O_3 interface. This fact prevents a straightforward correlation of the measured heat with the strength of the σ-dative bonds formed. In these circumstances, calorimetric and spectroscopic data cannot be simply correlated. The lack of correlation reveals that the interaction at the gas–solid interface may be more complicated than expected.

A supplementary proof that something different from a plain σ-coordination occurs at the CO/Al_2O_3 interface is shown in Fig. 5, that compares optical and volumetric isotherms of CO adsorbed on δ,θ-Al_2O_3 773. Both optical and volumetric isotherms are normalized to the unit surface area. The total optical isotherm was resolved into two individual components, a high-frequency species (2212–2210 cm^{-1}, that was termed species *B*, [16]), and a low frequency one (2200–2199 cm^{-1}, termed species *A* [16]). It has to be noted that the volumetric isotherm (intrinsically representative of all contributions) does not run parallel to the total optical isotherm, as one would expect on the basis of previous studies on *group IV* metal oxides and on the assumption that the Lambert–Beer law also holds in heterogeneous systems (see Refs. [10,24–27]). Indeed, on increasing CO pressures, the

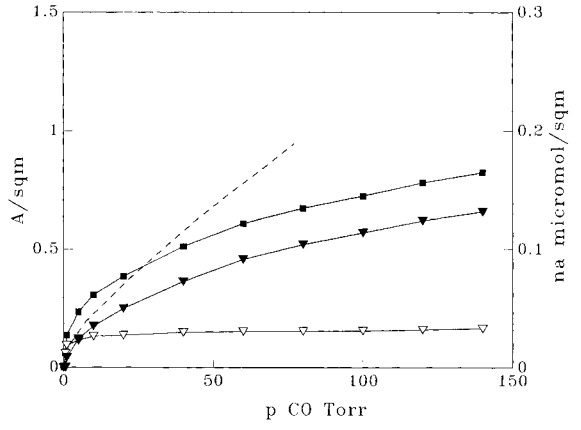

Fig. 5. Optical isotherms of CO adsorbed on δ,θ-Al_2O_3 773 at $T\approx300$ K: (■) total; (▼) species *A*, (▽) species *B* compared with the volumetric isotherm obtained at $T=303$ K (- - -).

volumetric isotherm keeps growing abnormally with respect to the optical one. The effect appears clearly evident at $p_{CO}>20$ torr and was observed also in the case of the other alumina samples under study, both γ- and δ,θ-Al_2O_3. (The relative optical isotherms are not reported for the sake of brevity.) This fact confirms the suggestion arising from the calorimetric data, that something peculiar occurs at the CO/Al_2O_3 interface.

The unusual behavior of Al_2O_3, detected independently by both calorimetric and volumetric experiments, is not evident in a simple inspection of the ν_{CO} stretching frequency region of the IR spectrum. The fact that the adsorbed amounts increase with CO pressure more steeply than the integrated absorbances can be explained by accepting the idea that the volumetric/calorimetric and spectroscopic experiments are performed in conditions that are only nominally identical. In fact the temperature of the sample under the IR beam and the temperature of the sample in the calorimeter are certainly not the same. The calorimeter is kept isothermal at 303 K, whereas a gradient of temperature is created in the IR cell because of the heating of the sample under the IR beam. For this reason, additional IR spectra were recorded on a sample kept at a temperature as close as possible to 303 K (by cooling the cell in a liquid water/ice bath). The intensities of the IR band assigned to the formation of species *A* were found to increase significantly with respect to those of the same band recorded on the uncooled sample [47]. Moreover, by cooling the sample the optical isotherm becomes parallel to the volumetric one.

It is obvious that a relatively weak molecular adsorption such as the one of CO on CUS metal cations is depressed when the temperature increases, but the effect on species *A* is too dramatic to be associated only to this fact. Indeed, the intensity of the IR band assigned to the formation of species *B* was found to be affected insignificantly by the variation of the temperature, similarly to what was previously found for the CO species formed on the other metal oxides studied [10,11,25,27]. Species *A* are thus supposed to form on sites having peculiar features, i.e. on sites located on flat portions of regular low index planes in the proximity of strained Al–O groups. The temperature experienced by the sample in the IR beam (i.e. the uncooled sample), most of the strained groups are likely to be rearranged in such a way that the CO adsorption is fastly inhibited.

The endothermic effect due to the reversible modification of the surface is slightly depressed by the presence in the alumina matrix of CUS cations other than Al^{3+}. For instance, the presence of low concentration of Ce^{4+} CUS cations modifies the behavior of pure alumina. In Fig. 6, the effect of the presence of cerium oxide dispersed on γ- and δ,θ-Al_2O_3 is illustrated. In Fig. 6(a) the volumetric data, and in Fig. 6(b and c) the calorimetric ones relative to the interaction of CO with γ- and δ,θ-Al_2O_3/CeO_2 673 and 773, respectively, are reported. All quantitative and energetic data are compared with those of the pure parent alumina samples, pretreated under the same conditions. In Fig. 6(a), the volumetric isotherms show that the presence of CUS Ce^{4+} cations increases in all cases the total amount of surface sites sufficiently acidic to bind CO at room temperature.

As for the energy of interaction, Fig. 6(b) compares the heat vs. coverage plots for γ-phase samples (both *pure* and *ceria-doped aluminas*) outgassed at 673 and 773 K. In the case of the *samples outgassed at* 673 K, it can be observed that the two curves are very similar, but for the initial heat of adsorption q_0 that is significantly higher for the *ceria-doped sample* than for *pure alumina* ($q_0\approx50$ and ≈40 kJ/mol, respectively). In contrast, in the case of γ-Al_2O_3 and γ-Al_2O_3/CeO_2 outgassed at 773 K, q_0 is nearly the same for the two systems, but the decrease of the curve is somewhat less steep for the ceria-doped sample. This indicates that

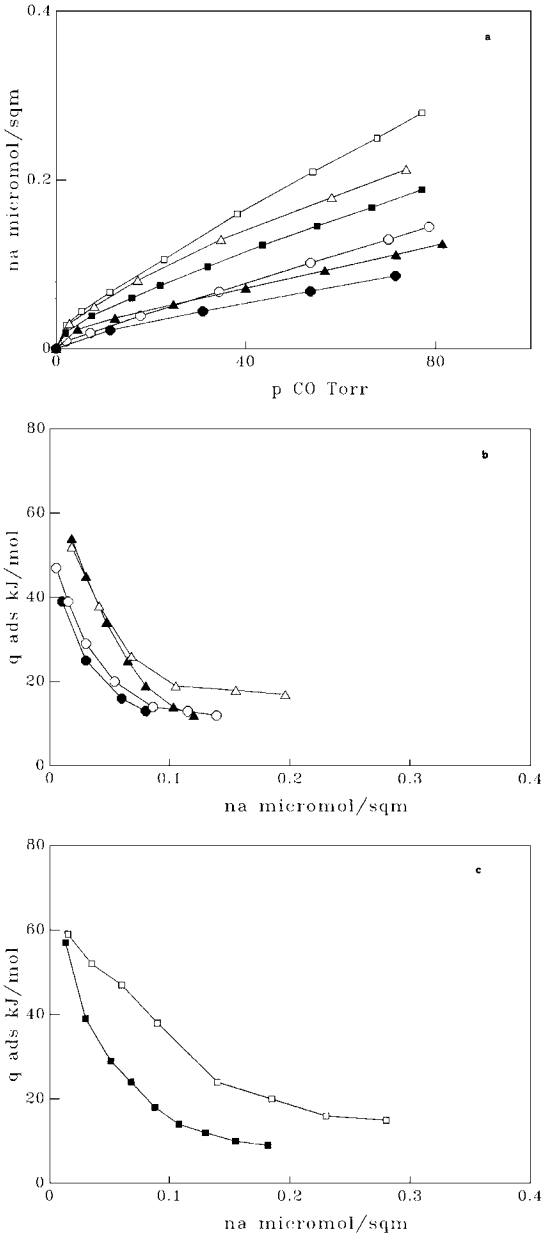

Fig. 6. (a) Adsorption volumetric isotherms of CO at 303 K on γ-Al_2O_3 outgassed at 673 K (●), on γ-Al_2O_3 outgassed at 773 K (▲) and on δ,θ-Al_2O_3 (■) outgassed at 773 K compared with the same samples doped with CeO_2 3% w/w outgassed at the same temperatures: γ-Al_2O_3/CeO_2 673 (○), γ-Al_2O_3/CeO_2 773 (△) and δ,θ-Al_2O_3/CeO_2 773 (□). (b) Heat of adsorption of CO on γ-Al_2O_3 673 (●) and 773 (▲) and the *ceria-doped* corresponding samples −673 (○) and −773 (△). (c) Heat of adsorption as a function of the CO uptake on δ,θ-Al_2O_3 773 (■) and the *ceria-doped* corresponding sample −773 (□).

the presence of Ce^{4+} cations tends to inhibit the endothermic effect associated with the surface modification. This fact is far more evident by comparing δ,θ-Al_2O_3 and δ,θ-Al_2O_3/CeO_2 773 samples, whose heat of interaction vs. coverage plots are reported in Fig. 6(c). The curves relative to pure and ceria-doped aluminas start more or less at the same q_0 value, but the decrease of the curve with coverage is smoother in the latter case. The presence of an abundant family of acidic sites of intermediate strength (q_{ads} ≈50–35 kJ/mol) is clearly evident.

Fig. 7 shows the IR spectra of CO adsorbed on *ceria-doped* γ- and δ,θ-Al_2O_3 in comparison with *pure* Al_2O_3. By inspection of the figure, it can be easily noted that: (i) in all cases a new band at lower ν_{CO} frequency appears; it is centered at 2175 cm^{-1} for γ-Al_2O_3/CeO_2 673 and 773, and at 2184 cm^{-1} for δ, θ-Al_2O_3/CeO_2 773. This band can be reasonably ascribed to CO adspecies formed on CUS Ce^{4+} cations, even if the stretching frequency of CO

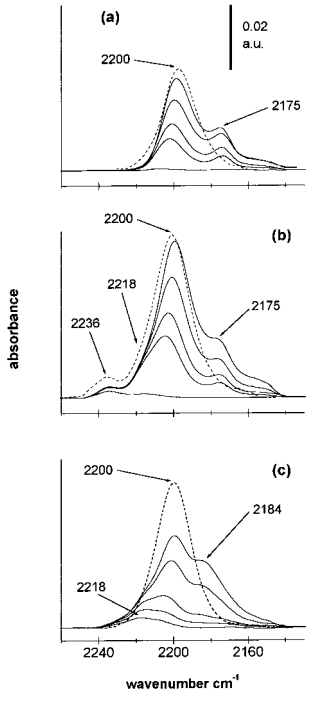

Fig. 7. IR spectra of CO adsorbed at T ≈300 K on γ-Al_2O_3/CeO_2 673 (a), on γ-Al_2O_3/CeO_2 773 (b) and on δ,θ-Al_2O_3/CeO_2 773 (c) at increasing CO pressure (1–150 torr) compared with the correspondent IR-bands on the pristine *pure* γ- and δ,θ-Al_2O_3, at p_{CO} ≈150 torr (- - -).

adsorbed on CUS Ce^{4+} on pure CeO_2 is lower, ranging in the interval 2150–2170 cm^{-1} [12,17]; (ii) for the γ-Al_2O_3/CeO_2 673 sample the low frequency CO species termed *A* is the only Al^{3+}/CO species present and is as abundant as in pure alumina, indicating that the Ce^{4+}/CO species do not form at the expense of the species *A*; (iii) for γ-Al_2O_3/CeO_2 773 the spectral pattern of pure alumina is not significantly modified: the 2175 cm^{-1} species (CO/Ce^{4+}) keeps growing, but not at the expense of the 2199 cm^{-1} one (CO/Al^{3+}, species *A*), in that the intensity of the latter band is not significantly depressed in ceria-doped alumina; (iv) in the case of δ,θ-Al_2O_3/CeO_2 773 the stretching frequency of CO adsorbed on Ce^{4+} cations is higher than in the γ-Al_2O_3/CeO_2 773 case, indicating that the electron accepting power of the CUS Ce^{4+} cations is remarkably increased. In addition, the presence of Ce^{4+} cations seems to stabilize the most acidic CUS Al^{3+} cations, as indicated by the appearance of shoulders in the high frequency side of the main CO/Al^{3+} *A* band. These shoulders can be ascribed to the formation of CO adspecies termed *B* and *C* [16]. Thus, from both calorimetric and spectroscopic results it is evident that a new family of Lewis-acidic sites is created on adding ceria to alumina. From an energetic point of view, it can be noted that the presence at the surface of CUS Ce^{4+} cations alternating to CUS Al^{3+} depresses (mostly in the δ,θ-Al_2O_3/CeO_2 773 sample) the endothermic modification of the surface occurring upon CO uptake (see the heat vs. coverage plot in Fig. 6(b) and (c)). CUS Ce^{4+} sites are less acidic than CUS Al^{3+} ones, as suggested by the smaller blue-shift of the ν_{CO} band (2175–2184 cm^{-1} instead of 2199–2200 cm^{-1}). Thus, the overall acidity of the sample is increased in terms of acid sites population, but not in terms of acidic strength.

The *heat of interaction*, measured at increasing CO coverage for δ,θ-Al_2O_3/CeO_2 773 is higher than the one measured for pure δ,θ-Al_2O_3, but we are not able to assign precisely the heat values to the adsorption of CO on Ce^{4+} cations, in that the measured heat might not be entirely due to the σ-coordination of CO. However, using the measured frequency value (2175–2184 cm^{-1}) and the correlation between ν_{CO} and $\Delta_{ads}H$, as previously reported [10,35], permits the formation of a σ-dative bond between CO and CUS Ce^{4+} cations to be assigned a value in the 35–45 kJ/mol range. These latter sites, when dispersed in an alumina matrix, can thus be considered as Lewis-acidic sites of medium strength.

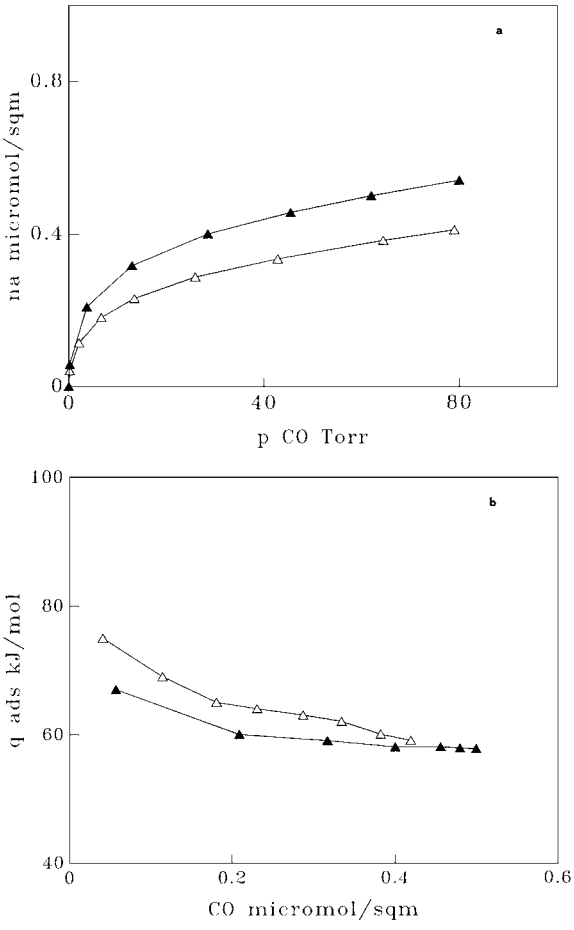

Fig. 8. (a) Adsorption volumetric isotherms of CO at 303 K on the *pure* tetragonal *t*-ZrO_2 723 (▲) and on the *sulfated t*-ZrO_2/SO_4 723 (△). (b) Heat of adsorption as a function of CO uptake on the samples described in (a).

In Fig. 8(a) the volumetric isotherms and in Fig. 8(b) the calorimetric data of CO adsorbed on a *tetragonal* ZrO_2 sample and on the correspondent *sulfated* one are reported. The catalytic activity of the sulfated zirconia sample in the low temperature (453 K) isomerization of *n*-butane was tested [48], and the results obtained allow to consider this sample as a *solid superacid*.

In Fig. 8(a) the adsorbed amounts are reported as a function of CO pressure for both pure *t*-ZrO_2 and sulfated *t*-ZrO_2/SO_4 outgassed at T=723 K. This out-

gassing temperature was chosen in order to reach a high dehydroxylation degree, but avoiding the sulfate decomposition that in vacuo starts at $T \geq 823$ K. The overall population of CO sites is lower for the sulfated sample, as expected, because sulfates occupy structural positions that belong to Zr^{4+} cations in the pure sample [49]. At p_{CO}=60 torr the population of strongly acidic sites in pure *t*-ZrO_2 is ca. 0.30 per square nanometer. From the Langmuir-like isotherm it can be roughly estimated that, at the completion of the monolayer, the population should be ca. 30% more abundant, i.e. it roughly involves ≈0.4 CO sites/nm^2. On the sulfated *t*-ZrO_2/SO_4 the population at p_{CO}=60 torr is only 0.21 CO sites/nm^2, and the monolayer is estimated to involve ≈0.27 CO sites/nm^2.

In Fig. 8(b), the heat of adsorption vs. CO coverage for both *sulfated* and *unsulfated* *t*-ZrO_2 samples are reported. The initial heat of adsorption of CO on *sulfated* *t*-ZrO_2/SO_4 is definitely higher than on *pure* *t*-ZrO_2. The q_0 value is >80 kJ/mol for the *sulfated* system and ≈70 kJ/mol for the *unsulfated* one. The curve of the sulfated sample remains higher than that of the pure sample over the whole coverage range examined, but the two curves tend to merge at increasing coverages. This indicates that the major difference between the two samples is to be ascribed to the presence on sulfated zirconia of a very few strong Lewis sites. These strongly acidic sites are created by the presence of charge-withdrawing sulfate groups that increase the electron-accepting capacity of the CUS Zr^{4+} cations [49].

In Fig. 9, the IR spectra of CO adsorbed on the two zirconia samples are reported as a function of increasing CO pressure. The spectra consist, in both cases, of a single broad and asymmetric band. For the *pure zirconia* sample the band is located at ν_{CO}=2202 cm^{-1} at low CO pressure, and moves to lower frequencies with increasing coverage (ν_{CO}=2194 cm^{-1} at p_{CO} ≈150 torr). For the *sulfated sample* the ν_{CO} values are 2206 cm^{-1} at low CO pressure and 2197 cm^{-1} at p_{CO} ≈150 torr. The increase of the ν_{CO} blue-shift as a consequence of the presence of sulfate groups, though definitely small, is consistent with the higher heats of adsorption measured.

By comparing the populations of the sites on *pure tetragonal zirconia* and on *pure monoclinic zirconia* (see Fig. 1(a) and Fig. 8(a)) it can be noted that on *m*-

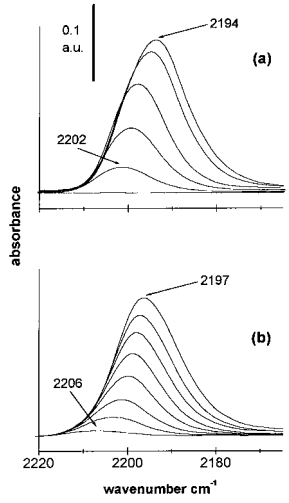

Fig. 9. IR spectra of CO adsorbed at T ≈300 K on the pure tetragonal *t*-ZrO_2 723 (a) and on the *sulfated* *t*-ZrO_2/SO_4 723 (b), at increasing CO pressure (1–150 torr).

ZrO_2 the overall population of CUS Zr^{4+}, sufficiently acidic to bind CO at r.t., is larger than on *t*-ZrO_2. For the *monoclinic* sample the population of acidic sites at p_{CO}=60 torr is 0.50 CO sites/nm^2, and the monolayer can be estimated to involve ≈0.65 CO sites/nm^2, against ≈0.4 sites/nm^2 estimated for the *tetragonal* sample. The difference is remarkable, and could be ascribed to different reasons. First, the outgassing temperature of the two samples was significantly different (673 K for *m*-ZrO_2 and 723 K for *t*-ZrO_2), and thus the hydration state was not comparable. However, the volumetric data indicate that the number of CO sites per unit surface area is much higher on *m*-ZrO_2 673 than on *t*-ZrO_2 723, i.e. on the sample dehydrated at a lower temperature. Second, the preliminary calcination temperature of the two samples was quite different. It was 673 K for *m*-ZrO_2 and 873 K for *t*-ZrO_2, so that the morphology of the two powdery systems (size and shape of the microparticles, amounts of structural defects etc.) could be different. HRTEM images (not reported for the sake of brevity) show that the two powdery samples are made up of nanosized crystallites whose dimension lies in the 10–20 nm range for *m*-ZrO_2 [50,51] and somewhat smaller for *t*-ZrO_2 (5–15 nm) [51]. The microparticles exhibit a disc-like shape with roundish contour and poorly defined edges, with a consequent abundance of crystallographically defective configurations, where a

higher coordinative unsaturation is expected for the exposed cations. The specific surface area of the two samples is also nearly the same, ≈85 m^2/g. So, the reasons for differences in the population of acidic sites cannot be found in the morphological and textural features of the two samples, that are quite similar. Structural reasons must be invoked. Computer graphics models reported in Ref. [51] seem to confirm this suggestion. The Lewis-acidic sites, more abundant on *monoclinic* zirconia, are somehow less strong than on the *tetragonal* one. In fact, q_0 is ≈60 kJ/mol in the former case and ≈70 kJ/mol in the latter one.

As for the strong Lewis acidity, attributed to sulfated zirconia, the strength of the sites is certainly quite high. CUS Zr^{4+} cations located in the proximity of sulfate groups show a significantly increased electron accepting power, but they are far from being the most acidic sites that can be found in the metal oxides class of compounds. For instance, as clearly shown in Ref. [44], the Lewis-acidic strength of a few sites present on a δ,θ-Al_2O_3 sample outgassed at high temperature (1023 K) is much higher ($q_0 \geq 90$ kJ/mol) than that exhibited by the *t*-ZrO_2/SO_4 specimen discussed in the present work. The initial heats of adsorption of CO on the various systems illustrated in the present work have values that are comparable to the q_0 value of *t*-ZrO_2/SO_4. This means that other features, complementary to the strong Lewis acidity, make the sulfated zirconia a *solid superacid*. These features have been extensively discussed in a recent paper [44].

4. Conclusions

The Lewis acidity of non-d/d^0 metal oxides can be fruitfully described through the combined use of adsorption microcalorimetry and IR spectroscopy in studying the room temperature adsorption of carbon monoxide. In general, both adsorption enthalpy and blue-shift of the stretching frequency of adsorbed CO can be taken as reasonable measures of the strength of the Lewis-acidic sites, provided that only a plain σ-coordination occurs at the surface site. Indeed, a correlation does exist between the two parameters. However, in some cases, namely for pure Al_2O_3 systems, processes other than a plain σ-coordination can occur at the CO/metal oxide interface, resulting in a measured heat inclusive of different energetic contributions. The calorimetric data are thus not simply correlated to the spectroscopic data, but suggest a complex process that occurs upon contact of CO with the surface. The population of the acidic sites (per unit surface area) as well as the distribution of their energy strongly depends not only on the chemical nature of the metal oxide and the activation conditions, but also on the different crystal structure of the metal oxide, and on the presence of cationic or anionic dopants.

Acknowledgements

The authors gratefully acknowledge the Italian "Consiglio Nazionale delle Ricerche (CNR)" for financial support (Comitato Nazionale per le Ricerche Tecnologiche; Contributo di ricerca N. 94.00544.CT11, Effect of form on the surface chemistry of finely divided solids).

References

[1] P.C. Gravelle, Adv. Catal., 22 (1972) 191.
[2] N. Cardona-Martinez, J.A. Dumesic, Adv. Catal., 38 (1992) 149.
[3] A. Auroux, in: Méthodes Thermiques, Calorimetrie, Analyse Thermique Differentielle, Thermo-gravimetrie in Les techniques physiques d'étude des catalyseurs Ed. Technip, Institut de Recherches sur la Catalyse, 1988, Chap. 24, 823.
[4] B. Fubini, (a) Rev Gén Thermique, 18(209) (1979), 297; (b) Thermochimica Acta 135 (1988) 19.
[5] B. Fubini, V. Bolis, F.S. Stone, M. Bailes, Solid State Ionics 32/33 (1989) 258.
[6] M. O'Neil, J. Phillips, J. Phys. Chem., 91 (1987) 2867.
[7] L.C. Jozefowicz, H.G. Karge, E.N. Coker, J. Phys. Chem., 98 (1994) 8053.
[8] M. Cabrejas Manchado, J.M. Guil, A. Pérez Masiá, A. Ruiz Paniego, J.M. Trejo Menayo, Langmuir 10 (1994) 685.
[9] J.A. Dunne, R. Mariwala, M. Rao, S. Sircar, R.J. Gorte, A.L. Myers, Langmuir, 12 (1996) 5888.
[10] V. Bolis, B. Fubini, E. Garrone, C. Morterra, J. Chem. Soc. Faraday Trans. I 85 (1989) 1383.
[11] V. Bolis, C. Morterra, M. Volante, L. Orio, B. Fubini, Langmuir, 6 (1990) 695.
[12] C. Morterra, V. Bolis, G. Magnacca, J. Chem. Soc. Faraday Trans. 92 (1996) 1991.
[13] V. Bolis, B. Fubini, E. Giamello, A. Reller, J. Chem. Soc. Faraday Trans. I 85 (1989) 855.
[14] V. Bolis, B. Fubini, E. Giamello, Mater. Chem. Phys, 29 (1991) 153.

[15] C. Morterra, G. Cerrato, V. Bolis, B. Fubini, Spectrochimica Acta, 49A (1993) 1269.
[16] C. Morterra, V. Bolis, G. Magnacca, Langmuir, 10 (1994) 1812.
[17] C. Morterra, G. Magnacca, V. Bolis, G. Cerrato, M. Baricco, A. Giachello, M. Fucale, in: Catalysis and Automotive Pollution Control III (Elsevier Science), 96 (1995) 361.
[18] J. Sauer, P. Ugliengo, E. Garrone, V.R. Saunders, Chem. Rev., 94 (1994) 2095.
[19] (a) B. Fubini, V. Bolis, A. Cavenago, P. Ugliengo, J. Chem. Soc. Faraday Trans., 88 (1992) 277; (b) B. Fubini, V. Bolis, A. Cavenago, E. Garrone, P. Ugliengo, Langmuir, 9 (1993) 2712.
[20] B. Rosenblum, A.H. Nethercot Jr., C.H. Townes, Phys. Rev. 109 (1958) 400.
[21] (a) L.H. Little, C.H. Amberg, Can. J. Chem., 40 (1962) 1997; (b) K. Nakamoto, in: Infrared and Raman Spectra of Inorganic and Cooordination Compounds (3rd edn. Wiley New York) 1978, p. 279.
[22] N.S. Hush, M.L. Williams, J. Molec. Spectroscopy 50 (1974) 349.
[23] A.M. Ferrari, P. Ugliengo, E. Garrone, J. Chem. Phys., 105 (1996) 4129.
[24] C. Morterra, E. Garrone, V. Bolis, B. Fubini, Spectrochimica Acta, 43A (1987) 1577.
[25] E. Garrone, V. Bolis, B. Fubini, C. Morterra, Langmuir, 5 (1989) 892.
[26] V. Bolis, B. Fubini, E. Garrone, C. Morterra, P. Ugliengo, J. Chem. Soc. Faraday Trans. 88 (1992) 391.
[27] V. Bolis, C. Morterra, B. Fubini, P. Ugliengo, E. Garrone, Langmuir 9 (1993) 1521.
[28] B. Fubini, V. Bolis, E. Giamello, Thermochimica Acta 85 (1985) 23.
[29] D.A. Seanor, C.H. Amberg, J. Chem. Phys 42 (1965) 2967.
[30] T.L. Brown, D.J. Davensbourg, Inorg. Chem. 6 (1967) 971.
[31] E. Escalona Platero, D. Scarano, G. Spoto, A. Zecchina, Faraday Discussions Chem. Soc., 80 (1985) 1.
[32] A. Zecchina, S. Bordiga, C. Lamberti, G. Spoto, L. Carnelli, C. Otero Areán, J. Phys. Chem. 98 (1994) 9577.
[33] T.A. Egerton, F.S. Stone, J. Chem. Soc., Faraday Trans. I, 69 (1973) 22.
[34] E.A. Paukshtis, R.I. Soltanov, E.N. Yourchenko, React. Kinet. Catal. Lett., 16 (1981) 93.
[35] V. Bolis, B. Fubini, E. Garrone, E. Giamello, C. Morterra, in: Structure and Reactivity of Surfaces, C. Morterra, A. Zecchina, G. Costa (Eds.), Elsevier Sci. Pub., B.V. Amsterdam, 1989, p. 159.
[36] (a) N.D. Parkins, in: Chemisorption and Catalysis, P. Hepple (Ed.), Inst. of Petroleum, London, 1970, p. 150; (b) Knözinger, H., Adv. Catal, 25 (1976) 184; (c) K. Tanabe, in: Catalysis, Science and Technology, J.R. Anderson, M. Boudart (Eds.), C. Springer Verlag, Berlin, 2 (1982) 23.
[37] G.A.M., Hussein, N. Sheppard, M.I. Zaki, R.B. Fahim, J. Chem. Soc. Faraday Trans I., 85 (1989) 1723; 87 (1991) 2655; 87 (1991) 2661.
[38] (a) Y. Nakamo, T. Iizuka, H. Hattori, K. Tanabe, J. Catal., 57 (1979), 1; (b) N.B. Jackson, J.G. Ekerdt, J. Catal., 101 (1986) 90; J. Kondo, H. Abe, Y. Sakata, K. Maruya, K. Domen, T. Onoshi, J. Chem. Soc. Faraday Trans I., 84 (1988) 511.
[39] (a) B. Gates, J.R. Katzer, G.C.A. Schmit, Chemistry of Catalytic Processes, Mc Graw Hill New York, 1979, Chapt. 3; (b) K. Tanabe, in: Catalysis, Science and Technology, J.R. Anderson, M. Boudart, (Eds.), C. Springer Verlag, Berlin, 1982, p. 239.
[40] (a) A.F. Divell, R.R. Rajaran, H.A. Shaw, T.J. Truex, in: Catalysis and Automotive Pollution Control II, A. Crucq (Ed.), Elsevier Science, Amsterdam, 1991, p. 39; (b) J.G. Nunan, H.J. Robota, M.J. Cohn, S.A. Bradley, in: Catalysis and Automotive Pollution Control II, A. Crucq (Ed.), Elsevier Science, Amsterdam 1991, p. 221.
[41] (a) M. Hino, S. Kobayashi, K. Arata, J. Am. Chem. Soc., 101 (1979) 6435; (b) M. Hino, K. Arata, J. Chem. Soc., Chem Commun., 101 (1980) 851; (c) M. Misono, Y. Okuhara, Chem. Tech, 1993, Nov. 23.
[42] (a) C. Morterra, G. Cerrato, F. Pinna, M. Signoretto, G. Strukul, J. Catal, 149 (1994), 181; (b) F. Pinna, M. Signoretto, G. Strukul, G. Cerrato, C. Morterra, Catal. Lett., 26 (1994) 335.
[43] C. Morterra, G. Cerrato, V. Bolis, C. Lamberti, L. Ferroni, L. Montanaro, J. Chem. Soc. Faraday Trans., I 91 (1995) 113.
[44] C. Morterra, G. Cerrato, V. Bolis, S. Di Ciero, M. Signoretto, J. Chem. Soc. Faraday Trans., 93 (1997) 1179.
[45] C. Morterra, G. Magnacca, Catal. Today, 27 (1996) 497.
[46] L. Marchese, S. Bordiga, S. Coluccia, G. Martra, A. Zecchina, J. Chem. Soc., Faraday Trans., 89 (1993) 3483.
[47] V. Bolis, G. Magnacca, C. Morterra, in preparation.
[48] C. Morterra, G. Cerrato, M. Signoretto, Catal. Lett., 41 (1996) 101.
[49] V. Bolis, G. Magnacca, G. Cerrato, C. Morterra, Langmuir 13 (1997) 888.
[50] C. Morterra, V. Bolis, B. Fubini, L. Orio, T.B. Williams, Surface Science 251 (1991) 540.
[51] C. Morterra, G. Cerrato, L. Ferroni, L. Montanaro, Mater. Chem. and Phys. 37 (1994) 243.